Supplementary Material for

Characterization of chain alignment at buried interfaces using Mueller matrix spectroscopy

*Bryan H. Smith,[1] Renxuan Xie,[1] Wonho Lee,[1] Dipendra Adhikari,[2,3] Nikolas J. Podraza[2,3] and Enrique D. Gomez[1,4,5]**

[1]Department of Chemical Engineering, The Pennsylvania State University, University Park, PA 16802

[2]Department of Physics and Astronomy, University of Toledo, Toledo, OH 43606

[3]Wright Center for Photovoltaics Innovation and Commercialization, University of Toledo, Toledo, OH 43606

[4]Department of Materials Science and Engineering, The Pennsylvania State University, University Park, PA 16802

[5]Materials Research Institute, The Pennsylvania State University, University Park, PA 16802

*email: edg12@psu.edu

Contents

Experimental

Materials

Regioregular poly(3-hexylthiophene) (RR P3HT, M_w = 17.5 kg/mol, M_n = 14.7 kg/mol, regioregularity = 95%) was synthesized according to methods previously outlined.[1] RR P3HT and regiorandom poly(3-hexylthiophene) (RRa P3HT, Sigma Aldrich, M_w = 108 kg/mol, M_n = 33.5 kg/mol, regioregularity = 58%) were characterized using dynamic light scattering (DLS), ^{1}H nuclear magnetic resonance (NMR), and gas permeation chromatography (GPC).

Mueller matrix Spectroscopy

Films for optical characterization were spun cast onto UV-ozone treated silicon with approximately 2 nm native oxide substrates at 1000 rpm for 60 seconds from solutions prepared from anhydrous chlorobenzene (Sigma Aldrich, 99.8%). The concentration was varied to vary the film thickness. Solutions were stirred at room temperature for approximately 12 hours in a nitrogen-purged glovebox. Films were thermally annealed at 165 °C immediately after casting for 12 hours unless noted otherwise.

Films were exposed to air for optical measurement which was conducted on a J.A. Woollam RC2 dual rotating compensator multichannel instrument collecting Mueller matrix spectra with a 30 second collection time per incident angle.[2] Data was collected and fit over the maximum 210-1690 nm range. RRa P3HT data was obtained and fit for 50°, 60°, and 70° incident angles, and RR P3HT data was obtained at 45°, 55°, 65° and 75°. RR P3HT data was fit at 45° and 75°. To collect data from multiple locations on a given film, the substrate was rotated 45°. All modeling was done with J.A. Woollam CompleteEASE software.

Mean Squared Error (MSE) Analysis

MSE values reported in this letter are calculated using Equation 1 where M_{exp} is the experimentally measured Mueller matrix element at a given wavelength, M_{fit} is the model Mueller matrix element at that wavelength, and n is the number of wavelengths data is collected at:

$$MSE = 1000 \times \frac{1}{n}\sum_{i=1}^{n}\sqrt{(M_{exp} - M_{fit})^2} \qquad (1)$$

The MSE calculated by CompleteEase includes the multiplication by 1000 and so this equation was used in all MSE calculations for consistency. Unless otherwise noted, MSE is calculated over the entire 210-1690 nm range, all incident angles fit, and every Mueller matrix element.

Thickness Values and Associated Error Bars

Total film thickness is taken to be the sum of each polymer layer in the model, plus half of the surface roughness if included. The error bars reported are a single standard deviation.

Modeling

Polymer optical properties were modeled with Gaussian and Tauc-Lorentz oscillators, with each set of optical properties represented by between 3 to 7 oscillators. Oscillators were added or removed as necessary to produce physically realistic results depending on what data was being fit. Generally, thinner films required fewer oscillators. The substrate in each model was accounted for using crystal silicon and native oxide optical properties[3] The native oxide thickness was not fit while modeling the polymer films and was held to a value determined from measurements of the the blank wafers. All other layer thicknesses were fit while modeling.

Surface roughness was modeled as a Bruggeman effective medium approximation (EMA) consisting of equal 0.5 material volume fractions of the top polymer layer optical properties and air. This layer was added at the top of the stack.

Static Light Scattering

The persistence length of P3HT was obtained from static light scattering experiments. Static light scattering was run on dilute solutions of RRa P3HT in chlorobenzene with multiple concentrations from 4.0 to 1.2 mg/ml. As shown in Figure 1, a Zimm plot is constructed using a Brookhaven BI-200SM SLS/DLS instrument over an angular range of 40˚ to 140˚ and a 641 nm diode laser. These solutions were stirred overnight in a glovebox and then filtered through 0.2 μm PVDF filters multiple times. Temperature was maintained at 30.0 ± 0.2 ˚C during the scattering experiment. The differential refractive index (*dn/dc*), which is used to calculate the optical constant (*K*), is determined to be 0.155 ml/g in our previous work.[4]

In Figure 1, the weight-average molecular weight (M_w) is simply the inverse of the common intercept of zero-angle and zero-concentration extrapolations, while the radius of gyration (R_g) is obtained from the slope of the zero-concentration extrapolation. In addition, evaluation of the second virial coefficient from the slope of the zero-angle extrapolation gives $A_2 \sim 10^{-4}$ cm^3 mol/g, suggesting that chlorobenzene is a moderate solvent for RRa P3HT close to the theta condition. Assuming a Gaussian coil conformation in a diluted P3HT/chlorobenzene solution, the persistence length (l_p) can then be calculated according to[5]

$$l_p = \frac{3(R_g)^2 M_0}{l_0 M_w}, \qquad (2)$$

where M_0 and l_0 is the molecular weight and the length of the repeat unit (i.e. 166 g/mol and 0.39 nm for P3HT), respectively. Based on the extrapolated M_w and R_g in Figure S1, l_p is calculated to be 3.1 ± 0.7 nm using Equation 2. According to our previously published data[4] for another batch of RRa P3HT, l_p is calculated to be 2.7 ± 0.4 nm. Therefore, by averaging these two results, the persistence length of RRa P3HT is determined to be 2.9 ± 0.4 nm, which is in close agreement with 2.8 nm predicted by the freely rotating chain model.[6]

Polarized Optical Microscopy

Polarized optical microscopy was carried out on an Olympus BX53 microscope at room temperature. Images were acquired both with and without crossed polarizers using a 20× objective lens. The intensity of each image was integrated using ImageJ software.

Supporting Figures and Tables

Table S1. Mueller matrix spectra collected for regiorandom P3HT. Various subsets of this data are considered for different analyses throughout the letter as indicated.

Approximate film thickness (nm)	Samples	Data collection locations per film
24	3	2
37	3	2
65	2	2
101	3	2
155	3	2
229	4	2

Table S2. Mueller matrix spectra collected for reioregular P3HT. Data was used to create an accurate model for regioregular P3HT that is used as an aligned bottom layer in the analysis of regiorandom P3HT, as described in the main text.

Approximate film thickness (nm)	Samples	Data collection locations per film
14	1	1
18	1	1
24	1	1
25	1	1
49	1	1

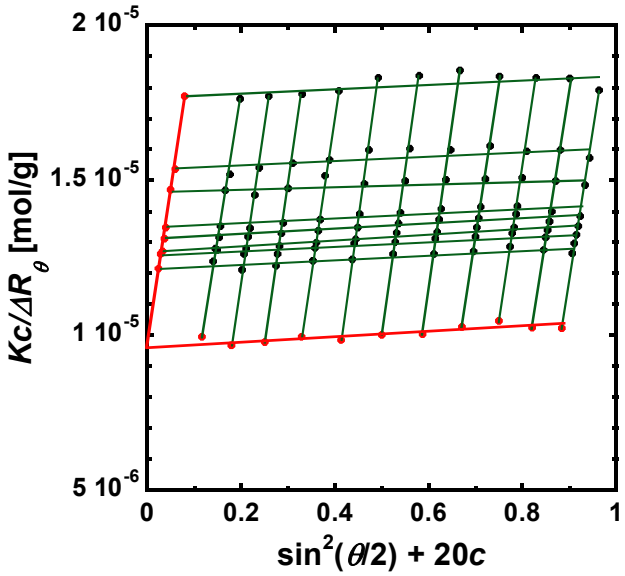

Figure S1. Zimm plot of regiorandom P3HT in chlorobenzene. (M_w: weight-average molecular weight, 108 ± 2 kg/mol; R_g: radius of gyration, 16.1 ± 1.8 nm; K: optical constants, 2.17×10^{-7} mol ml/g^2; c: polymer concentration (g/ml); ΔR_θ: Excess Rayleigh ratio; θ: scattering angle.)

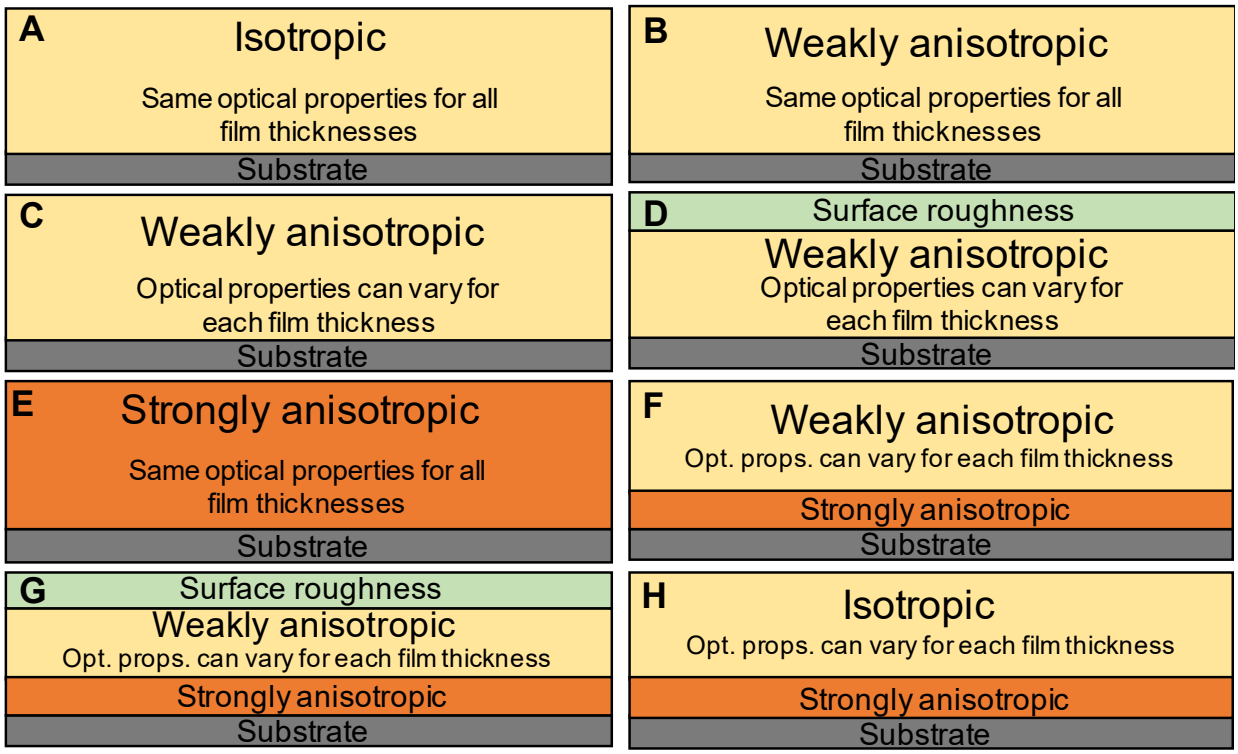

Figure S2. Summary of the models considered for application to fitting Mueller matrix spectra from P3HT films. Models shown in the order that they are referenced in the main text. Unless otherwise noted the model describes a RRa P3HT film . (A) Isotropic single layer model that does not account for surface roughness and in which the same optical propoerties are used for all film thicknesses. (B) Anisotropic single layer model that does not account for surface roughness and in which the same optical propoerties are used for all film thicknesses. (C) Anisotropic single layer model that does not account for surface roughness and in which the optical propoerties may vary for each film thickness. (D) Anisotropic single layer model that accounts for surface roughness and in which the same optical propoerties may vary for each film thickness. (E) Anisotropic single layer model that does not account for surface roughness and in which the same optical properties are used for all film thicknesses. This model describes RR P3HT. (F) Anisotropic two layer model that does not account for surface roughness. The weakly anisotropic layer optical properties can vary with film thickness, but the strongly anisotropic layer optical properties are fixed to those derived with Model E for each film thickness. (G) Anisotropic two layer model that accounts for surface roughness. The weakly anisotropic layer optical properties can vary with film thickness, but the strongly anisotropic layer optical properties are fixed to those derived with Model E for each film thickness. (H) Isotropic top two layer model that does not account for surface roughness. The isotropic layer optical properties can vary with film thickness, but the strongly anisotropic layer optical properties are fixed to those derived with Model E for each film thickness.

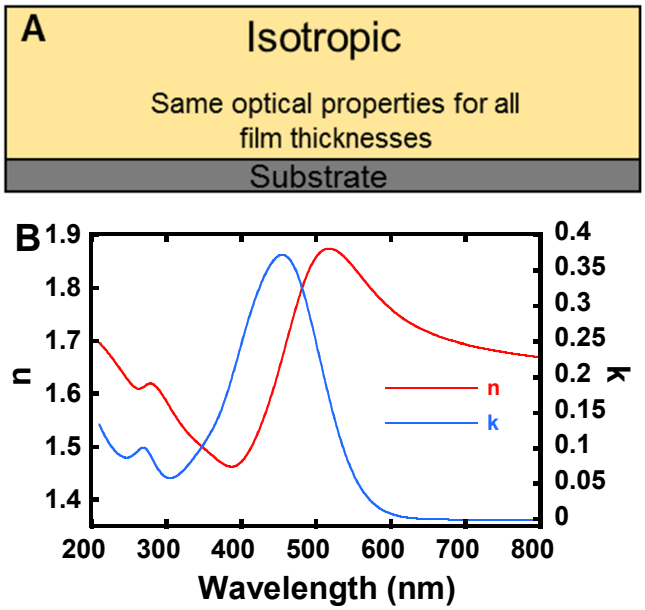

Figure S3. (A) Schematic showing a single layer isotropic model. The same set of optical properties, represented by the complex index of refraction ($N = n + ik$) describe films of all thickness. (B) Regiorandom P3HT optical properties derived from fitting a one-layer isotropic model to data in the 210-1690 nm range for a variety of film thicknesses (24-240 nm) all assumed to have the same optical properties.

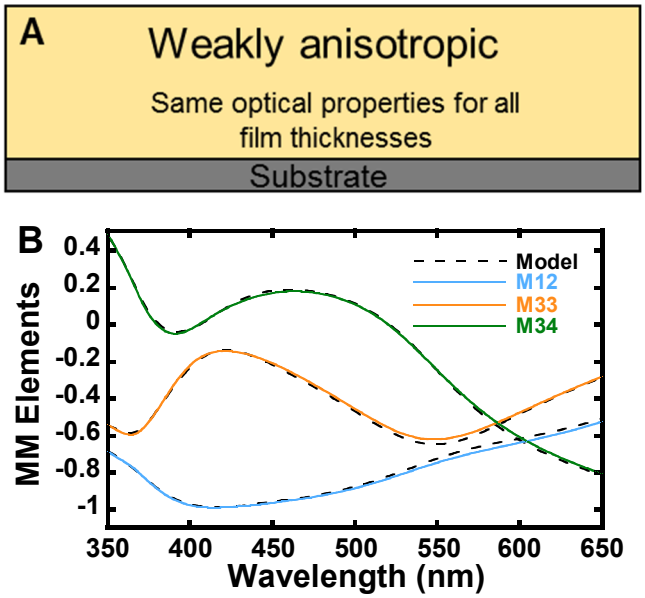

Figure S4. (A) Schematic showing a single layer anisotropic model. The optical properties describe films of all thicknesses. (B) Selected Mueller matrix elements for a 155 nm thick regiorandom P3HT film at 60° incident angle in the 350-650 nm range are shown as solid lines. A one-layer model shown as dashed lines was derived from fitting data in the 210-1690 nm wavelength range for a variety of film thicknesses (24-230 nm) with the same optical properties. The optical properties are assumed to be anisotropic which leads to a slightly improved fit and justifies adding further complexity to more accurately describe the film.

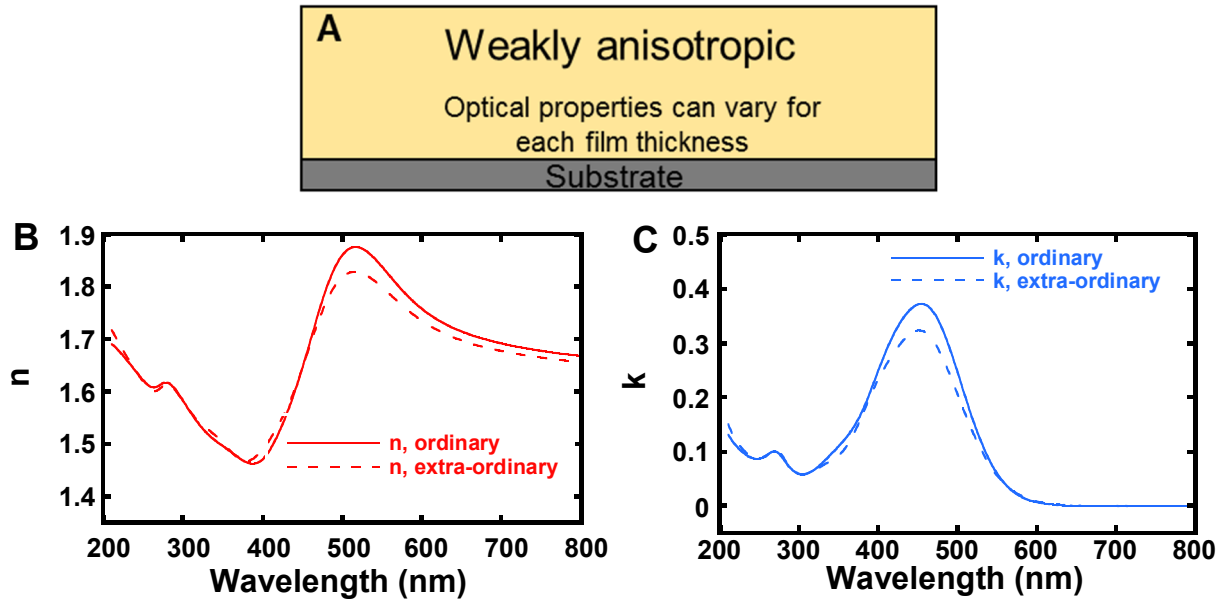

Figure S5. (A) Schematic showing a one-layer anisotropic model. The same set of optical properties describe films of all thickness. Regiorandom P3HT optical properties derived from fitting a one-layer anisotropic model to data in the 210-1690 nm range for a variety of film thicknesses (24-240 nm) all assumed to have the same optical properties. (B) Ordinary and extra-ordinary refractive index (*n*). (C) Ordinary and extra-ordinary extinction coefficient (*k*).

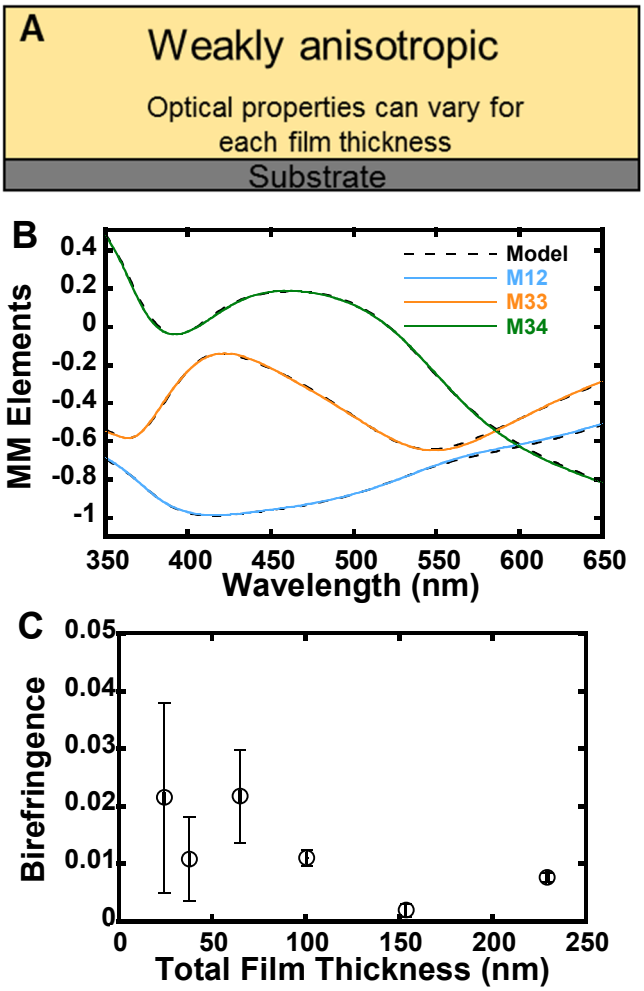

Figure S6. (A) Schematic showing a single layer anisotropic model. The optical properties may vary for each film thickness. (B) Selected Mueller matrix elements for a 155 nm thick regiorandom P3HT film at 60° incident angle in the 350-650 nm range shown as solid lines. A one-layer anisotropic model shown as dashed lines was derived from fitting data in the 210-1690 nm wavelength range for all 155 nm samples with the same optical properties. This fit improvement justifies considering models in which properties change with thickness. (C) Mean 1100 nm wavelength birefringence results from a single layer anisotropic model that does not account for surface roughness.

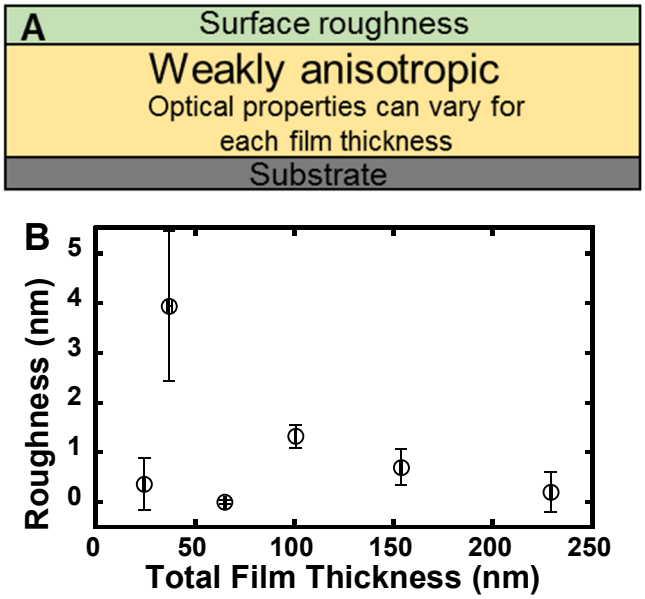

Figure S7. (A) Schematic showing a single layer anisotropic model with surface roughness. The optical properties can vary for each film thickness. (B) Mean surface roughness shown with standard deviation bars for regiorandom P3HT films of various thickness as determined in the single layer anisotropic model.

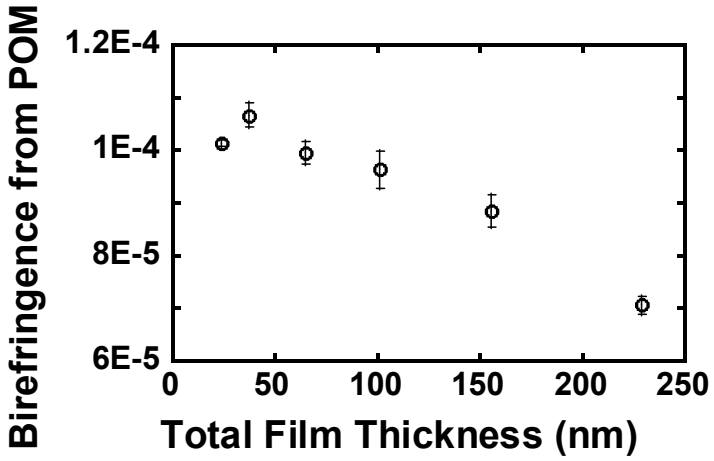

Figure S8. Polarized optical microscopy (POM) birefringence from RRa P3HT thin films of various thicknesses. Birefrignence is caclulated as the ratio of image intensities while polarizers are crossed to intensities from uncrossed images.

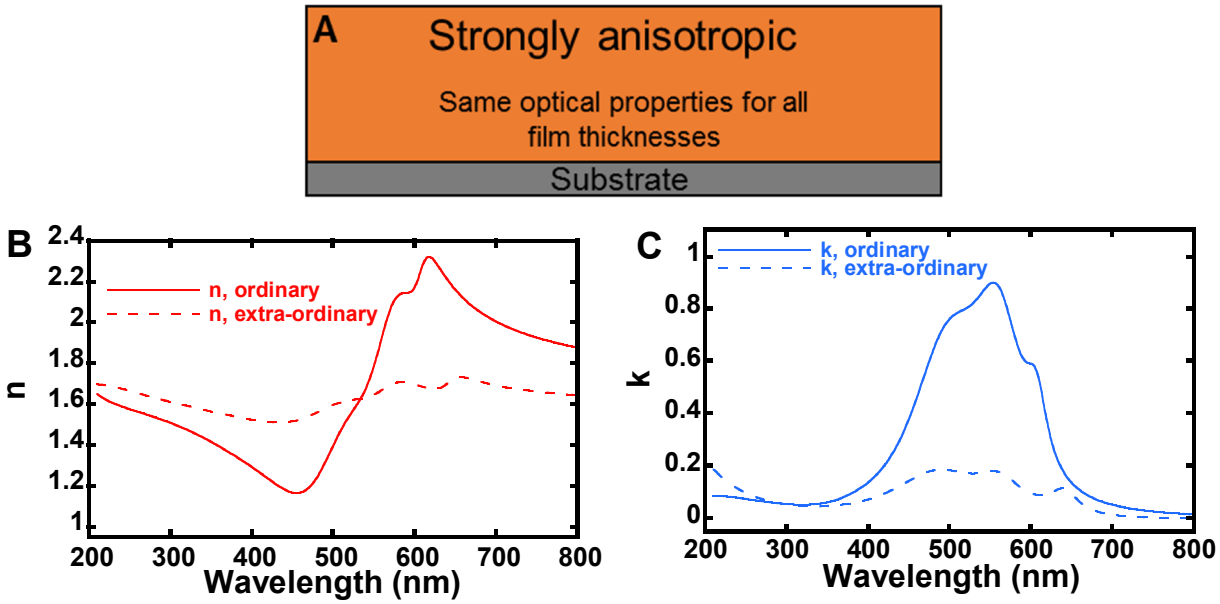

Figure S9. Regioregular P3HT optical properties derived from fitting a one-layer anisotropic model to data in the 210-1690 nm range for a variety of film thicknesses (14-49 nm) all assumed to have the same optical properties. These properties are used in the buried aligned interface layer for the two layer anisotropic models. (A) Schematic showing a model composed of a single layer that is strongly anisotropic. The optical properties are constant for all film thicknesses. (B) Ordinary and extra-ordinary refractive index (*n*). (C) Ordinary and extra-ordinary extinction coefficient (*k*).

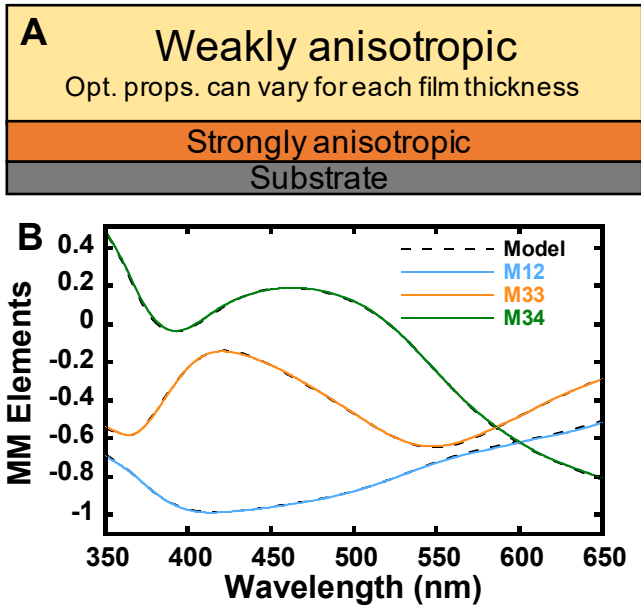

Figure S10. (A) Schematic showing a model with two anisotropic layers. The weakly anisotropic layer optical properties may vary for each film thickness while the strongly anisotropic layer optical properties do not. (B) Selected Mueller matrix elements for a 155 nm thick regiorandom P3HT film at 60° incident angle in the 350-650 nm range shown as solid lines. A two-layer anisotropic model shown as dashed lines was derived from fitting data in the 210-1690 nm wavelength range for all 155 nm samples with the same optical properties. This model fits the data slightly better than the similar one layer model.

Table S3. MSE in the 350-650 nm absorption region for selected Mueller elements (M12, M33, M34) for various models

Figure in which model is portrayed	MSE over 350-650 nm range
1	16.0
S4	10.7
S6	5.1
S9	3.8

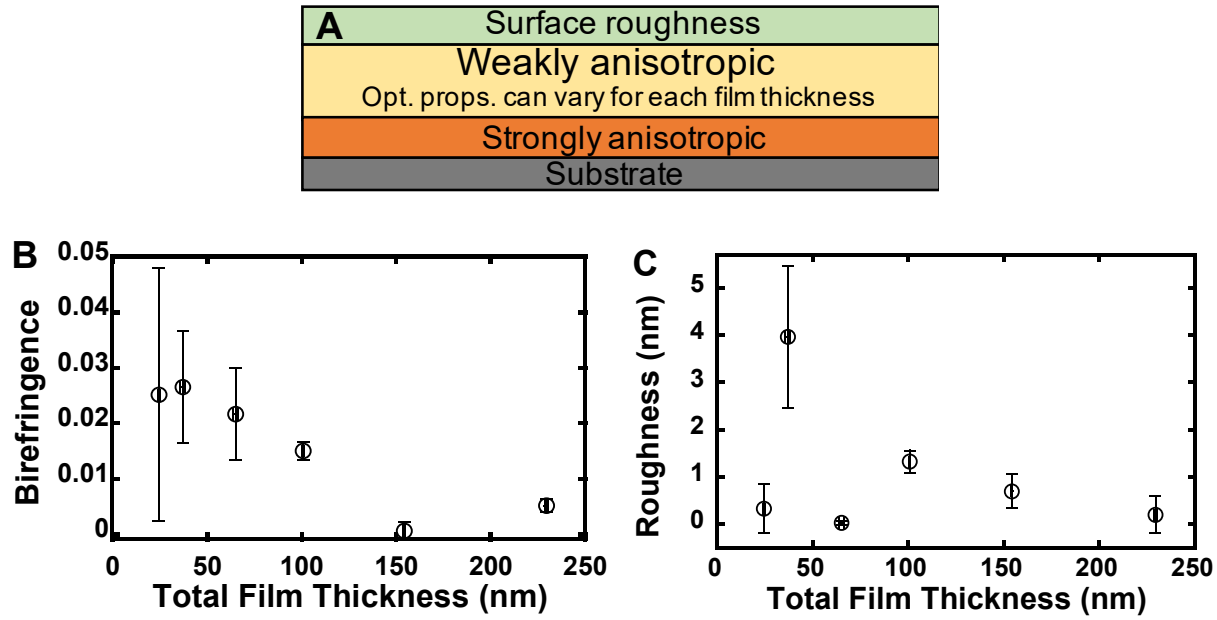

Figure S11. (A) Schematic showing a model with two anisotropic layers that includes surface roughness. The weakly anisotropic layer optical properties may vary for each film thickness while the strongly anisotropic layer optical properties do not. (B) Mean 1100 nm birefringence wavelength shown with standard deviation bars for regiorandom P3HT films of various thickness in the top layer as determined using a two-layer anisotropic model that accounts for surface roughness. The thickest two sets of samples show statistically significantly reduced birefringence as compared to thinner sets of samples. (C) Mean surface roughness shown with standard deviation bars for regiorandom P3HT films of various thickness as determined using the two layer anisotropic model.

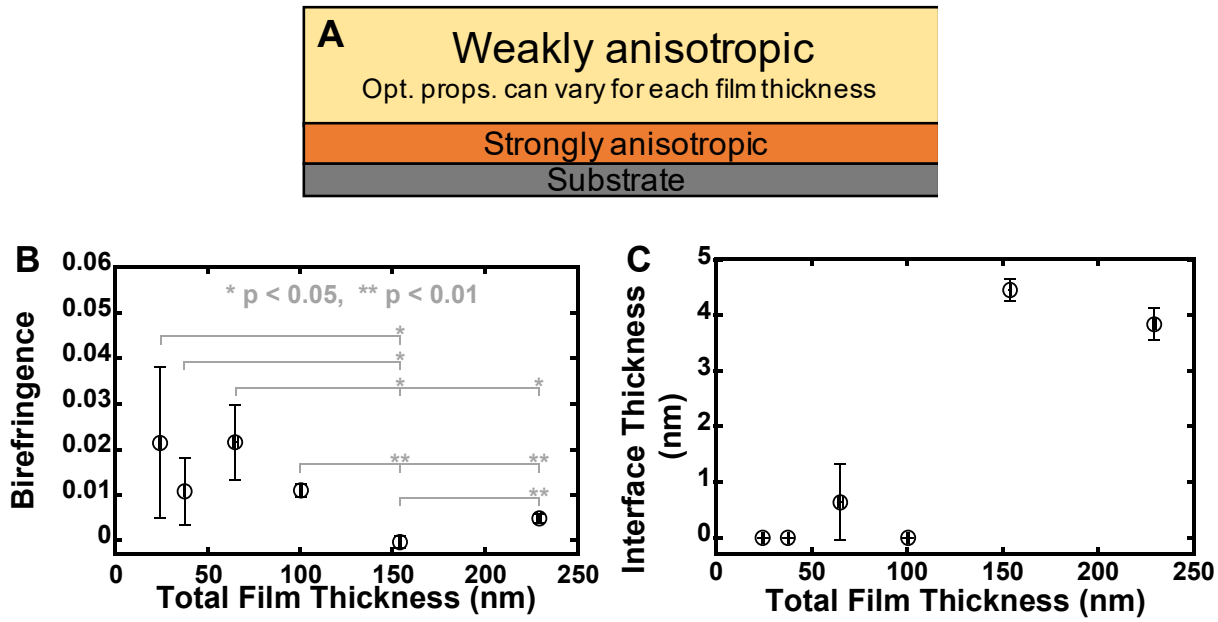

Figure S12. (A) Schematic showing a model with two anisotropic layers. The weakly anisotropic layer optical properties may vary for each film thickness while the strongly anisotropic layer optical properties do not. (B) Mean 1100 nm wavelength birefringence results for the top layer from a two-layer anisotropic model that does not account for surface roughness. The general trend in the data is similar to that of Figure S10, although the 38 nm data point has lower birefringence in this analysis. Statistically significant differences are found between the thickest two data points and thinner films as denoted on the graph. (C) Thickness of bottom layer (aligned buried layer) shown with standard deviation for regiorandom P3HT films of various thicknesses as determined using a two-layer anisotropic model that does not account for surface roughness.

Table S4. Comparison of one and two layer anisotropic models for 155 nm films

Model	Roughness (nm)	Mean 1100 nm wavelength birefringence	Mean bottom layer thickness (nm)	Mean MSE
One-layer with roughness	0.70	0.0028	0	4.81
One-layer without roughness	0	0.0019	0	4.82
Two-layer with roughness	0.69	0.0006	4.45	4.58
Two-layer without roughness	0	-0.0003	4.45	4.60

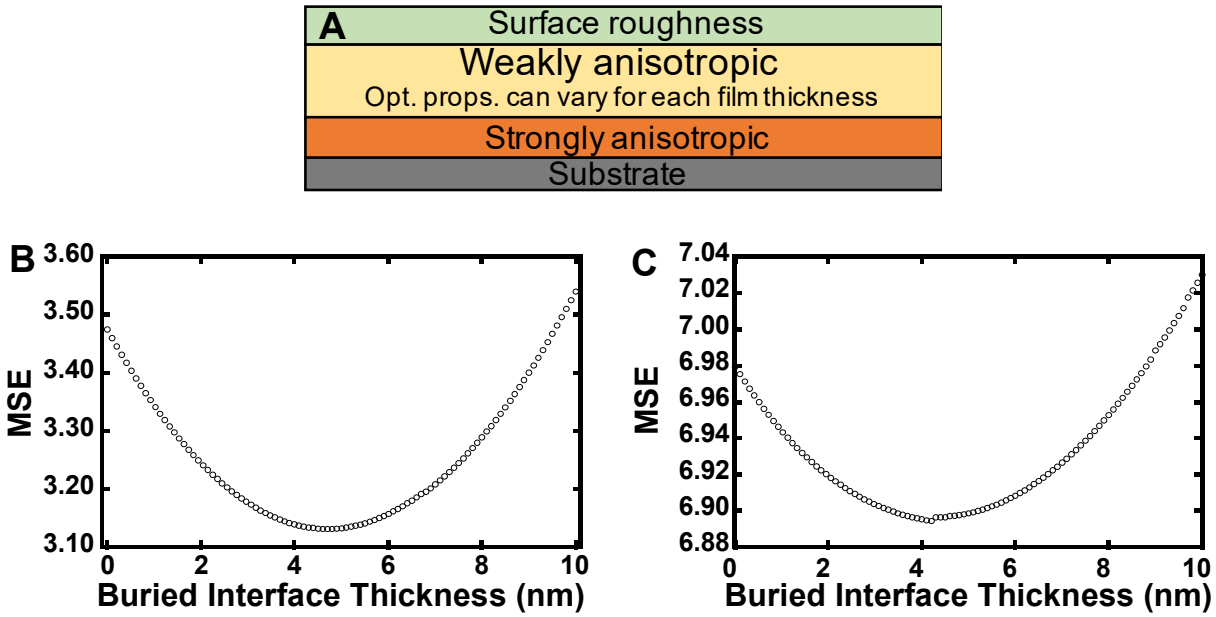

Figure S13. (A) Schematic of a two layer model that accounts for surface roughness. Parameter uniqueness tests on the bottom layer thickness for (B) a 155 nm film and (C) a 230 nm film fit with the two-layer anisotropic model that accounts for surface roughness. The presence of an obvious minimum in mean square error (MSE) is evidence that the thicknesses are meaningful.

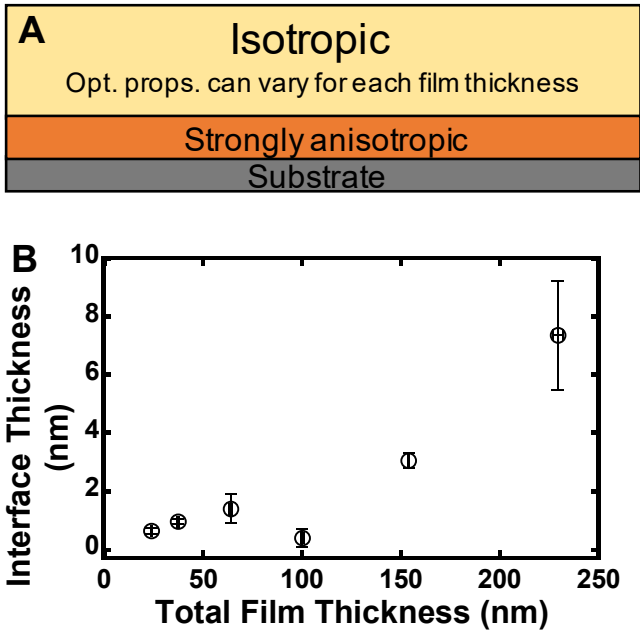

Figure S14. (A) Schematic of a two-layer model with an isotropic top layer that does not account for surface roughness. (B) Thickness of bottom layer (aligned buried layer) shown with standard deviation from regiorandom P3HT films of various thicknesses as determined using a two-layer (isotropic top) model that does not account for surface roughness. Although the fit quality is worse for this model than for the two-layer anisotropic model, the results are similar.

Table S5. Effect of annealing at 165 ºC for 12 hrs on RRa P3HT Mueller matrix spectroscopy results.

Total film thickness	Bottom layer thickness no anneal	Bottom layer thickness with anneal	Top layer 1100 nm birefringence no anneal	Top layer 1100 nm birefringence with anneal
38 nm film	0.0	0.0	0.023	0.014
152 nm film	6.7	4.5	0.02	-0.002

References

1. Lee, Y.; Aplan, M. P.; Seibers, Z. D.; Kilbey, S. M.; Wang, Q.; Gomez, E. D., Tuning the synthesis of fully conjugated block copolymers to minimize architectural heterogeneity. *Journal of Materials Chemistry A* **2017,** *5* (38), 20412-20421.
2. Chen, C.; An, I.; Ferreira, G. M.; Podraza, N. J.; Zapien, J. A.; Collins, R. W., Multichannel Mueller matrix ellipsometer based on the dual rotating compensator principle. *Thin Solid Films* **2004,** *455*, 14-23.
3. Herzinger, C. M.; Johs, B.; McGahan, W. A.; Woollam, J. A.; Paulson, W., Ellipsometric determination of optical constants for silicon and thermally grown silicon dioxide via a multi-sample, multi-wavelength, multi-angle investigation. *Journal of Applied Physics* **1998,** *83* (6), 3323-3336.
4. Xie, R.; Lee, Y.; Aplan, M. P.; Caggiano, N. J.; Müller, C.; Colby, R. H.; Gomez, E. D., Glass Transition Temperature of Conjugated Polymers by Oscillatory Shear Rheometry. *Macromolecules* **2017,** *50* (13), 5146-5154.
5. Hunt, M. L.; Newman, S.; Scheraga, H. A.; Flory, P. J., Dimensions and Hydrodynamic Properties of Cellulose Trinitrate Molecules in Dilute Solution. *The Journal of Physical Chemistry* **1956,** *60* (9), 1278-1290.
6. Kuei, B.; Gomez, E. D., Chain conformations and phase behavior of conjugated polymers. *Soft Matter* **2017,** *13* (1), 49-67.